Pergamon

Cement and Concrete Research 29 (1999) 507–514

CEMENT AND CONCRETE RESEARCH

Three-dimensional characterization of the pore structure of a simulated cement paste

Parviz Navi *, Christian Pignat

Swiss Federal Institute of Technology, Department of Material Sciences, Laboratory for Building Materials, MX-G Ecublens, CH-1015 Lausanne, Switzerland

Manuscript received 20 August 1998; accepted manuscript 23 October 1998

Abstract

Characterization of the pore structure of cement paste is of fundamental importance for understanding the mechanical and transport properties of cementitious materials. The influence of cement particle size distribution on the hydraulic radius and on the connectivity of the capillary pore space of hydrated tricalcium silicate (C_3S), simulated by an "integrated particle kinetics model" was studied previously. In this article, the pore size distribution of a simulated cement paste is determined by applying two different techniques: a two-dimensional numerical mercury intrusion technique and a morphological thinning and partitioning of void space technique. The results are discussed.

Keywords: Pore size distribution; Cement paste; Particle size distribution

Cement particles react with water and form a porous solid with micropores of various sizes. Understanding of the microstructure-property relationships of cement-based materials, as in any material, necessitates knowledge of microstructure at different levels. Through microscopic observation and analysis, one can simply obtain a two-dimensional (2D) quantitative image of hydrated cement paste microstructure, but it is extremely difficult to reconstruct an accurate three-dimensional (3D) microstructure from successive 2D images. Although certain microstructural aspects of cement paste, like phase volume fractions, are statistically the same in two and three dimensions, other structural features, like the connectivity or percolation of phases as well as the pore space size distributions, are considerably different. Various computer models have been developed in the last 10 years to represent the microstructure of cement paste development during hydration in 3D. Recently these models were reviewed by Bentz [1]. He classified these models into two categories. (1) A "continuum-based model" with spherical cement particles. The reason for this denomination is that the particles are described by their center and radius, corresponding to the nonhydrated core and the shells of hydration. In this approach the hydration process of cement particle is controlled by different mechanisms at different times. This type of simulation at the cement particle level first appeared in the pioneering work of Jennings and Johnson [2] and was continued in a similar way by Breugel [3]. (2) A digital-image–based model, developed by Bentz and Garboczi [4]. Their model allows the direct representation of multiphase and nonspherical cement particles, but unlike the continuum-based models it does not consider the different kinetics involved in the hydration process.

Based on the continuum representation approach, we implemented an integrated particle kinetics model for 3D simulation of the evolution of tricalcium silicate (C_3S) microstructure during hydration. The description of this model was given by Navi and Pignat [5,6]. In this model the effect of interparticle contacts and the accessibility of water on the rate of hydration and on the structure formation are taken into account explicitly. In this simulation the anhydrous particles of C_3S are considered to be spherical and possess a similar particle size distribution as Portland cement particles. The diameter of the particles can vary from 1 to 70 μm.

To demonstrate some of the results obtained by this simulation, a computational volume of $150 \times 150 \times 150$ μm^3 with both periodic and nonperiodic boundary conditions was considered. In this example the water-to-cement ratio is 0.4. At the start of the hydration the mixture consists of two phases: C_3S and water. After the hydration starts, the system contains five phases: C_3S, C-S-H, CH, water, and air. The air appears because of the "Le Châtelier" contraction. In this model the water and the air are considered to form the capillary porosity, and the water is assumed to be free water. At each step of the hydration, the overall degree of hydration,

* Corresponding author. Tel.: 41 21 693 2838; Fax: 41 21 693 58 00.

0008-8846/99/$–see front matter
PII: S0008-8846(98)00199-9

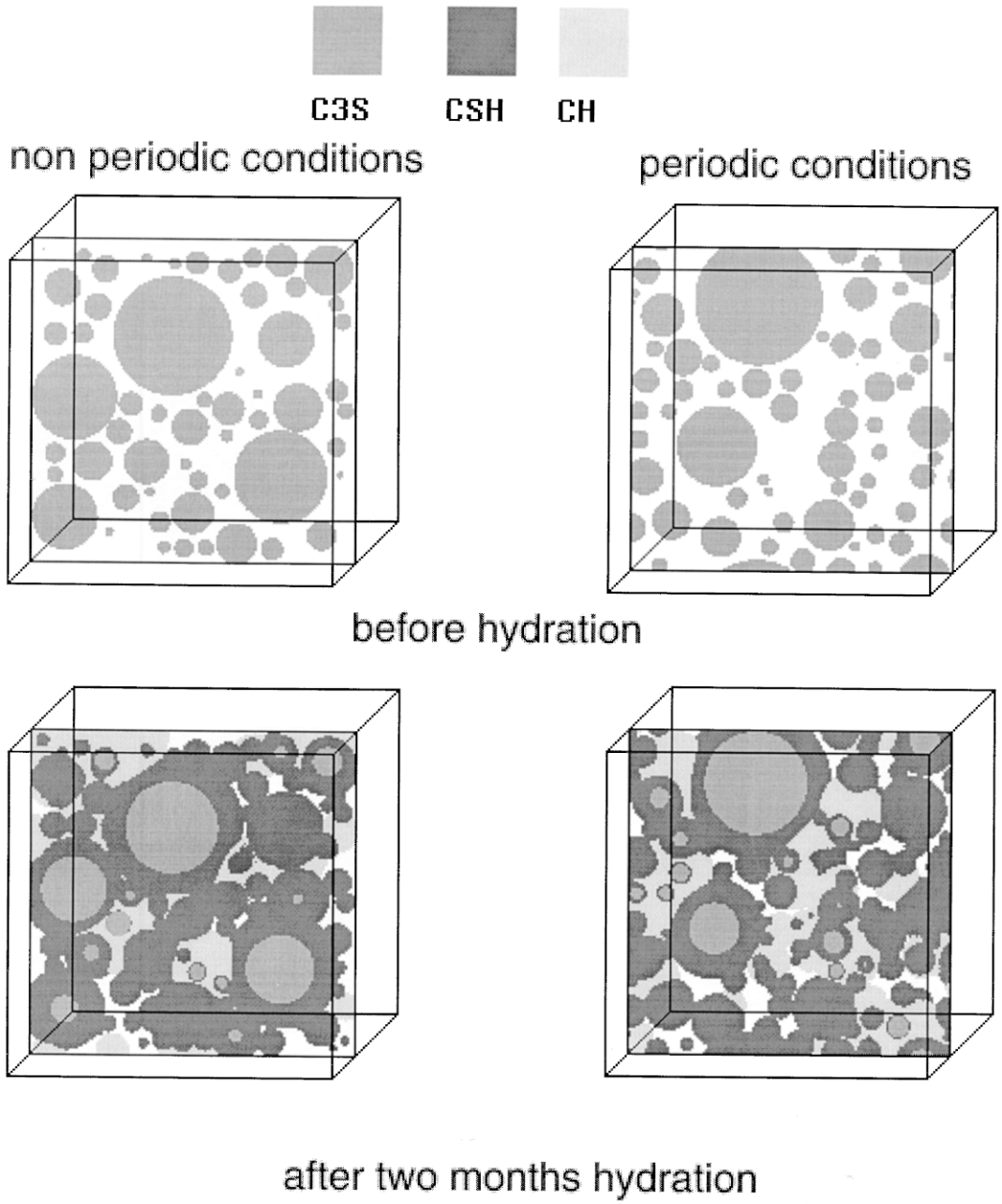

Fig. 1. Two-dimensional section of hydrated C_3S particles situated 50 μm from the computational volume surface, at t = 0 and t = 2 months.

the pore volume, the contact surfaces, and the hydraulic radius are computed and all data necessary for 3D graphical representation of the microstructure development of the cement paste are stored. Fig. 1 shows the 2D images at t = 0 and after 2 months of hydration of C_3S, under periodic and nonperiodic boundary conditions.

Hardened cement paste contains capillary pores whose size and volume vary during hydration. The dimension of pore spaces spans over five orders of magnitude in a scale varying from a few nanometers to several micrometers and mainly are interconnected, forming a highly complex network. Characterizing the pore structure of cement paste is of fundamental importance for understanding the mechanical properties and transport process of cementitious materials. A common approach to describe the pore space of the cement paste, in addition to its pore volume, is to represent the pore space as a distribution of pores of different sizes, as determined by mercury porosimetry or nitrogen adsorption measurements. In a classic mercury porosimetry experiment, the data are the incremental volumes of mercury that enter the pore space at each pressure increment.

The application of mercury porosimetry in practice is simple, but the interpretation of the data is difficult. A common and simple way to interpret these data is to consider the

pore spaces as nonintersecting cylindrical pores with various radii. The penetration pressure is the pressure required to force the mercury meniscus into the corresponding pore, where the relation between the capillary pressure P_c and the curvature C of the meniscus are given by the Laplace equation given in Eq. (1):

$$P_c = C\sigma \quad (1)$$

where σ is the surface tension, and $C = 2\cos\theta/r_t$, where r_t is the radius of the corresponding pore and θ is the contact angle between the interface and the solid surface.

Because the pore space of cement paste is complicated and composed of interconnected noncylindrical discrete pores, the derivation of pore size distributions from mercury porosimetry by a simple nonintersecting cylindrical pore model can give misleading results. Although many attempts have been made to give more realistic interpretations of mercury porosimetry data, e.g., using more sophisticated models based on grape features, the results still are not satisfactory [7].

The aim of this work at this stage is to determine the 3D pore size distribution of simulated cement paste. We applied two different techniques: a mercury intrusion technique (MIT) and a technique using morphological thinning and partitioning of the void space (MTPVS) [8]. The results obtained from these techniques are discussed. It is worthwhile to note that the application of MTPVS on a pore space for 2D or 3D is almost similar, but use of MIT on a 3D pore space is much more difficult than in 2D. In this article we will first give a brief description of these two numerical techniques and then compare the numerical results obtained from their application to 2D sections of simulated cement paste. Second, we will give the results obtained in 3D using the MTPVS technique.

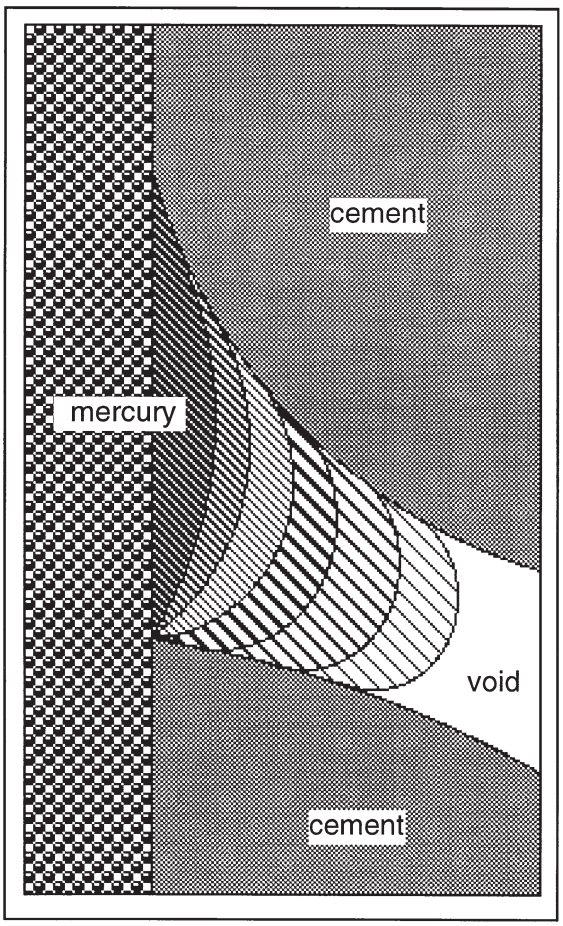

Fig. 2. Simulation of penetration of mercury from a portion of an edge of a 2D image under increasing pressure.

1. Numerical mercury porosimetry technique

In mercury intrusion, according to the Laplace equation, the pressure is proportional to the curvature of the mercury front meniscus. For a cylindrical pore the corresponding curvature is defined by a unique radius. For a noncylindrical pore, the corresponding curvature is a combination of two radii. This makes the numerical application of MIT to a simulated 3D pore space very difficult. Therefore, we applied this technique to a 2D porous structure where the meniscus is circular and the contact angle between solid and liquid is considered to be 180°.

Numerical application of MIT to 2D images follows a procedure similar to experiment. It starts from the edges of

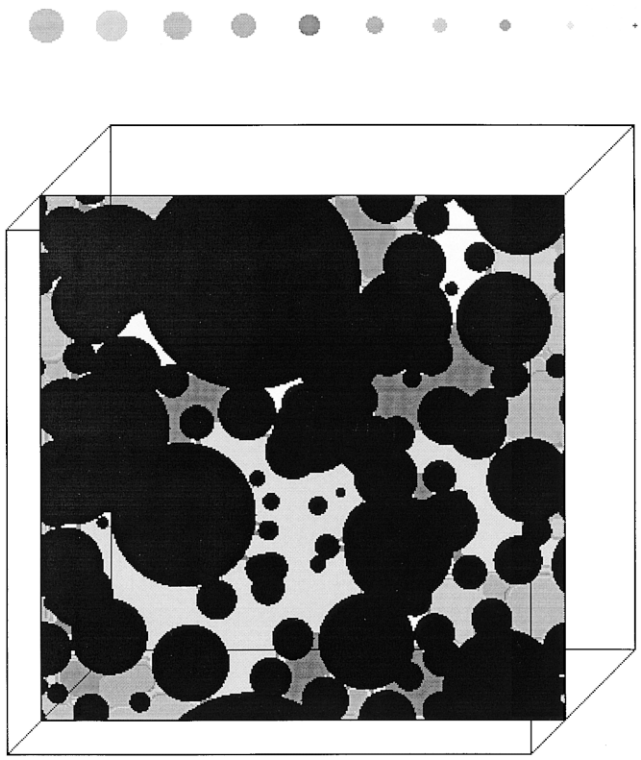

Fig. 3. Final penetration of mercury shown by different gray levels, each corresponding to minimum meniscus diameter for mercury penetration. The white color indicates the pores not penetrated by the minimum meniscus diameter of 0.5 μm.

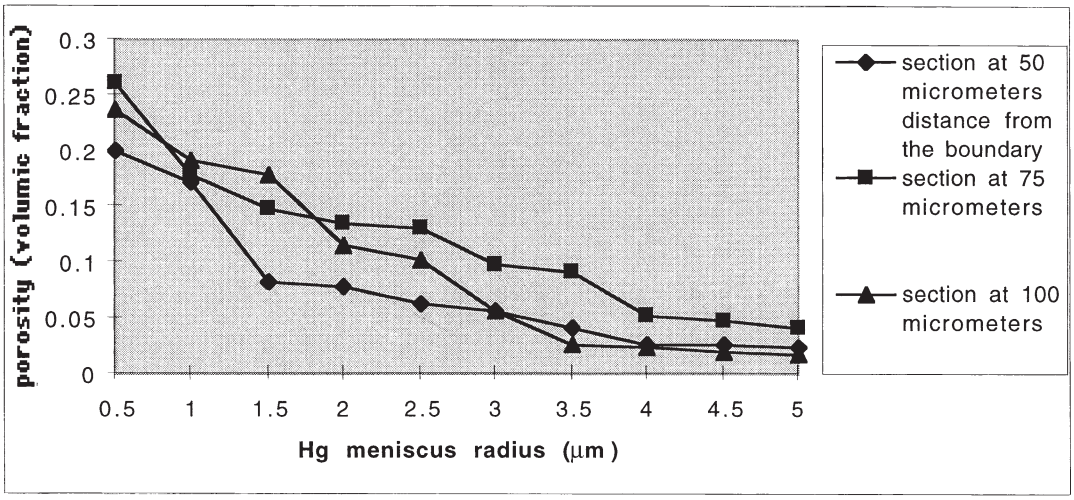

Fig. 4. Cumulative pore size distribution curves determined using the numerical mercury porosimetry technique on the 2D image.

the 2D image, filling the accessible pores with circles of a given diameter. This process of filling is carried out by reducing the diameter and is repeated until the pore space is filled out completely, as it shown in Fig. 2.

For each diameter the corresponding occupied surface is calculated. By varying the diameter, we can produce a complete intrusion curve for the considered microstructure. The result of such a numerical approach on a 2D slice of simulated hydrated cement is given in Fig. 3 In this example blocks represented in black are solids and the meniscus diameter varies with gray level from 5 to 0.5 μm.

The corresponding pore size distribution curves computed for three different slices at distances of 50, 75, and 100 μm from the boundary of computational volume are given in Fig. 4. Garboczi and Bentz [9] obtained, for a 2D microstructure, the pore size distribution using the same technique but applied to digital images.

2. MTPVS

This numerical approach is a variant of the morphological thinning method. It can be applied to a pore space demonstrated by images to partition the void space into a well-defined collection of individual pores. Each individual pore consists on a site bounded with interfaces with solid matrix, and by pore necks. A pore neck is defined as a plane where the hydraulic radius (area divided by its perimeter) has a local minimum. From the segmented pores several useful data such as pore size distribution curve and surface-to-perimeter ratio can be obtained. A general explication of this approach is given in Baldwin et al. [8]. We first applied this approach to a 2D structure of a pore space obtained from a 3D simulated microstructure of hydrated cement and then to a 3D porous structure.

Before this approach the pore structure had to be represented by regular pixels (or voxels for 3D images). Each pixel then will represent either a solid or a pore part. We should note that digitizing a continuum model and thus the result are dependent on the pixel size used. Because of the wide range of pore sizes in hydrated cement, it is evident that the size of the pixel has a strong influence on its pixel representation as well as on the pore size distribution. Using pixels having a very small size, one can obtain an accurate pore size distribution. Let us consider that at time t the 3D microstructure is simulated and a 2D slice is selected, and we intend to evaluate its pore size distribution with a pixel size d and a specimen size $a = n \times d$, where n is an integer.

The MTPVS technique consists of three stages: thinning, rebuilding, and computing equivalent radius of the individual pores. The thinning can be applied to an image when it

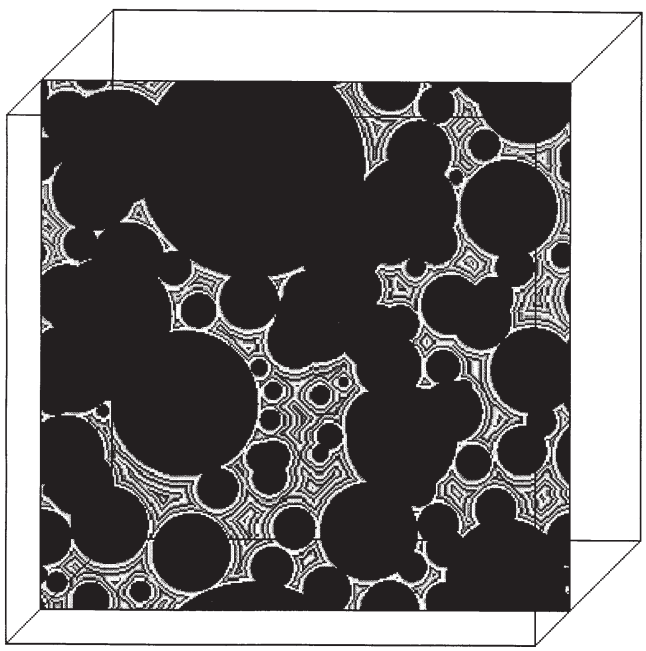

Fig. 5. Thinning of the 2D image of the pore space.

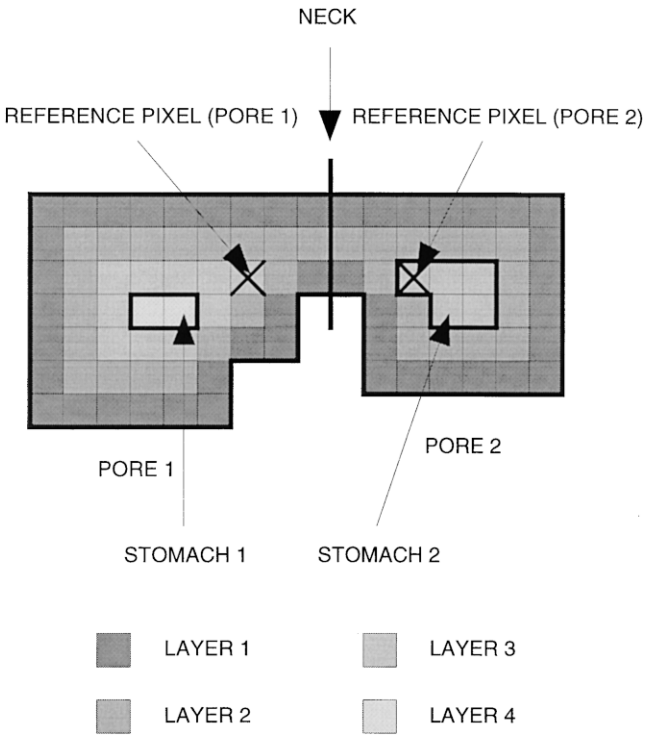

Fig. 6. Partitioning of the pore space into pores 1 and 2.

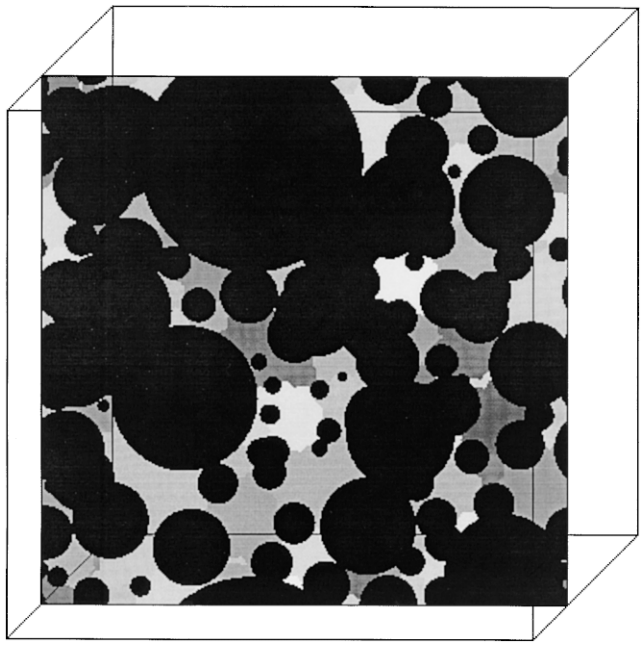

Fig. 7. Partitioning of the pore space of a 2D simulated cement pore. Each gray level shows an individual pore. The black color indicates the solid.

is represented by pixels or voxels. The aim of this operation is to replace the pore space with layers of pore pixels. The result of such thinning algorithm in a 2D image is shown in Fig. 5. During the morphological thinning, the pore pixels are removed from the surface of the pore space, layer by layer inward, giving each layer a number starting with one. This part of operation is called pores erosion or solids dilation.

When all the porous pixels are eroded, we start the second stage by rebuilding the pore space, layer by layer outward, beginning with the last eroded layer. This operation partitions the pore space into a set of individual pores. Each individual pore is identified by a discrete layer having a local maximum layer number (stomach) and a set of necks separating the pores. The necks and stomachs are defined as shown in Fig. 6, which illustrates an example of two distinct pores in 2D. Application of MTPVS technique is basically the same for both 2D and 3D. In Fig. 6 the stomach of pore 1 is made up of two pixels: layer 4, which is discrete and has local maximum layer number. The stomach of pore 2 is built of five pixels: layer 3, which is discrete and possesses local maximum layer number. Layer 2 does not represent

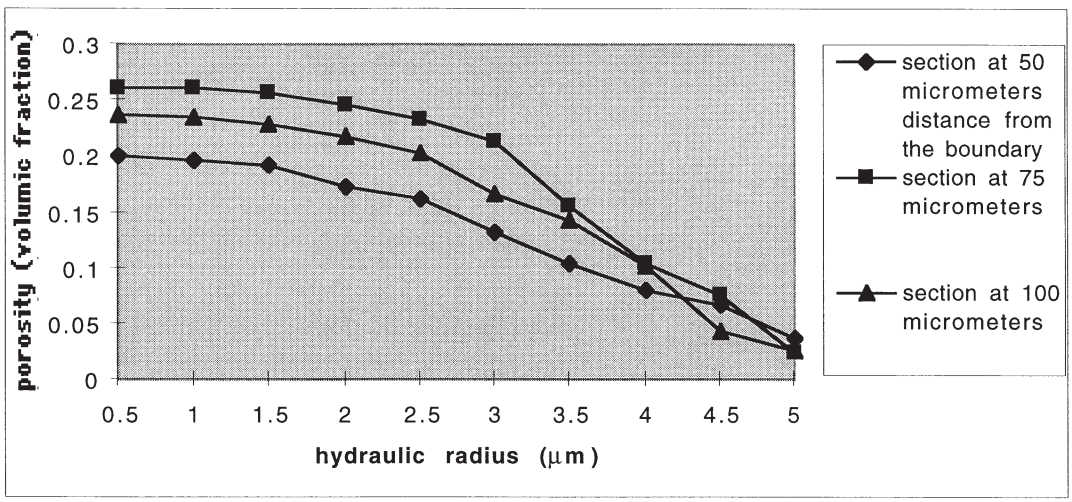

Fig. 8. Cumulative pore size distributions obtained for three sections at distances of 50, 75, and 100 μm from the boundary of computational volume using MTPVS.

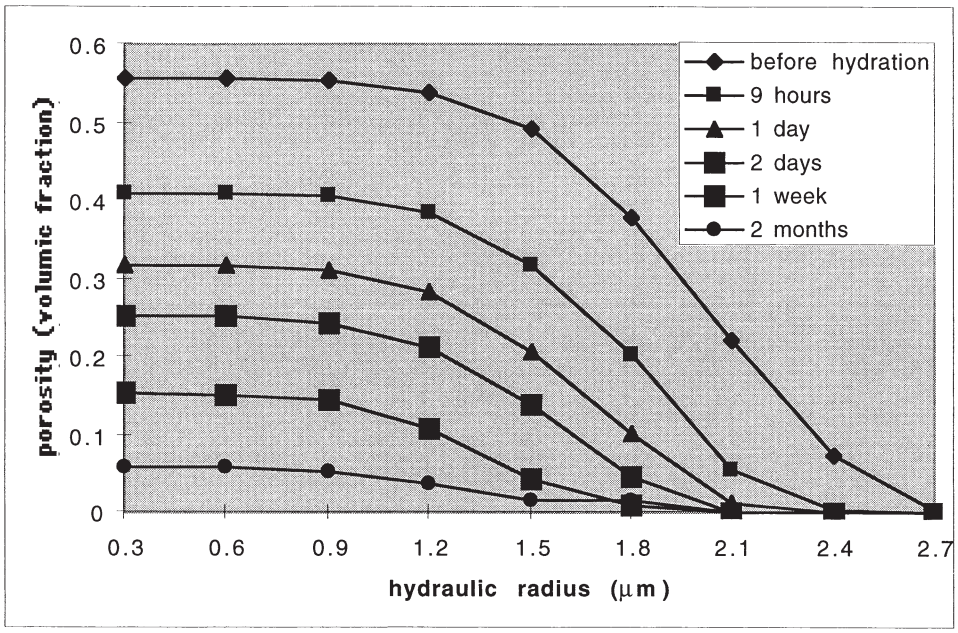

Fig. 9. Cumulative pore size distributions for a 3D specimen according to the MTPVS technique and at different hydration times.

any stomach. The neck pixels between the pores 1 and 2 are defined according to their equal distance with reference pixels of the pores. Reference pixels are the nearest pixels of the layer with the smallest layer number that separate the two pores. The line indicates the neck defined with respect to the two reference pixels of pores 1 and 2 in Fig. 6.

All statistics related to the characterization of pore space, such as pore size distribution, volume-to-surface ratio, etc., can readily be determined by this technique. To determine the pore size distribution curve, one should calculate for each pore its equivalent shape radius. For the purpose of comparison with the result obtained using mercury porosimetry, we defined a pore radius as being twice the ratio of surface to perimeter of the pore, which gives the exact radius for the pore if it were circular. Some hypothesis will be made in 3D computation. Individual pores will be considered merely spherical and the hydraulic radius of a 3D pore is calculated by multiplying by three the ratio of volume to surface, which corresponds to the real radius if the pore were spherical. We should note that there is no common accepted definition for equivalent shape radius. Our definition is more representative if the pore shape were closer to a circle or a sphere in 3D.

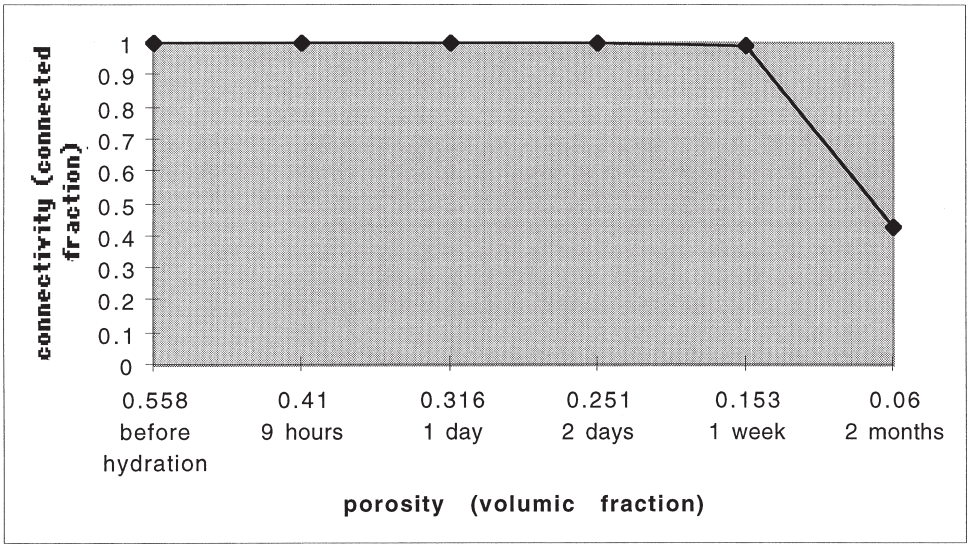

Fig. 10. Connectivity of the porosity for the different hydration times.

2.1 Pore size distribution curve using the MTPVS approach

Three 2D images identical to those studied with the numerical MIT were selected for application of the MTPVS approach. The result corresponding to Fig. 5 is given in Fig. 7, where each individual pore as defined before is shown by a different gray level.

Based on the definition given for the equivalent pore radius, we calculated the radius of each individual pore and its volume and surface. The cumulative pore size distributions of three 2D slices were computed and the corresponding curves are given in Fig. 8.

2.2 Three-dimensional characterization of the pore space of a simulated cement using MTPVS

It is not obvious how to apply the numerical MIT to a 3D pore structure to obtain the pore size distribution. As we explained previously, MTPVS can be applied readily to 3D and 2D images almost in the same manner. We applied this method to calculate the pore size distribution curve of our simulated hydrated cement at different hydration times. As an example, a $80 \times 80 \times 80$ μm^3 computational volume was considered. The C_3S grains were spherical and possessed a particle size distribution varying from 2 to 30 μm. The water-to-cement ratio was 0.4 and the number of grains was 1919. The pore space was represented by voxels 0.5 μm on a side. The cumulative pore size distributions of the pore spaces at different hydration times were calculated and are demonstrated in Fig. 9.

We also computed the connectivity of the pore spaces at different hydration steps using an algorithm proposed by Hoshen and Kapelman [10]. This algorithm has a bearing on 3D representation of a microstructure with successive 2D slices. It allows us to determine with precision the connectivity of pores, using voxels of a very small size [6]. The connectivity of the pore spaces represented by voxels 0.5 μm on a side and the porosity at different hydration times are given in Fig. 10

Illustrating the 3D image of partitioned pore space is difficult. Two-dimensional sections of the partitioned pore space for 3D numerical hydrated cement at different stages of hydration are given in Figs. 11–13. These figures show the evolution of individual pores and the solid parts (solid parts consist of C_3S and hydrated parts: C-S-H and CH) in a 1-week period using a section passing through the middle of

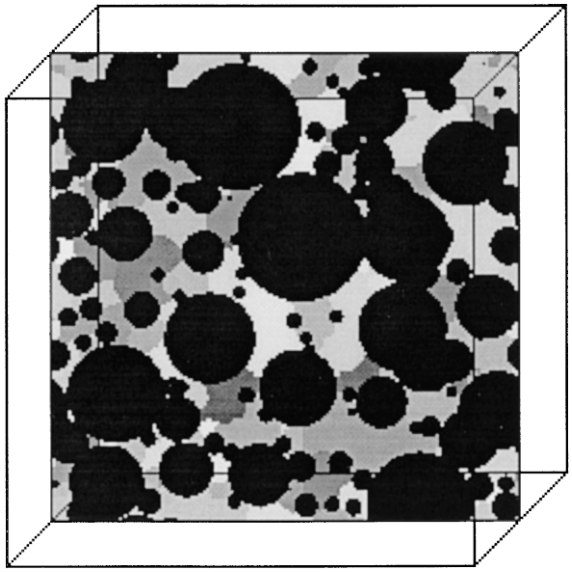

Fig. 12. Two-dimensional section in the middle of the specimen after 1 day of hydration.

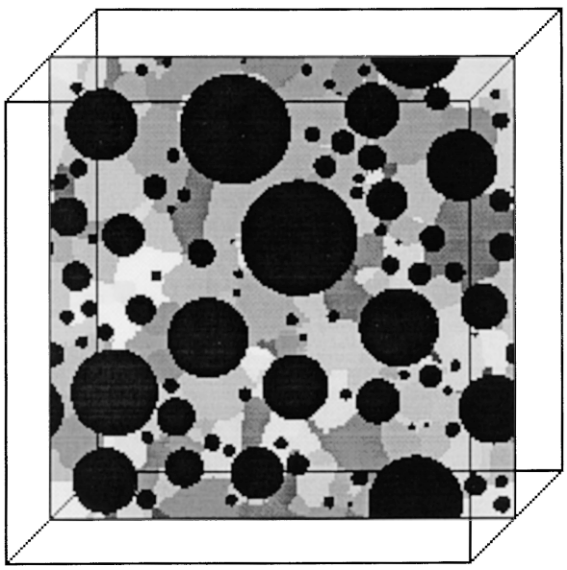

Fig. 11. Two-dimensional section in the middle of the specimen before hydration. The black color indicates the solid.

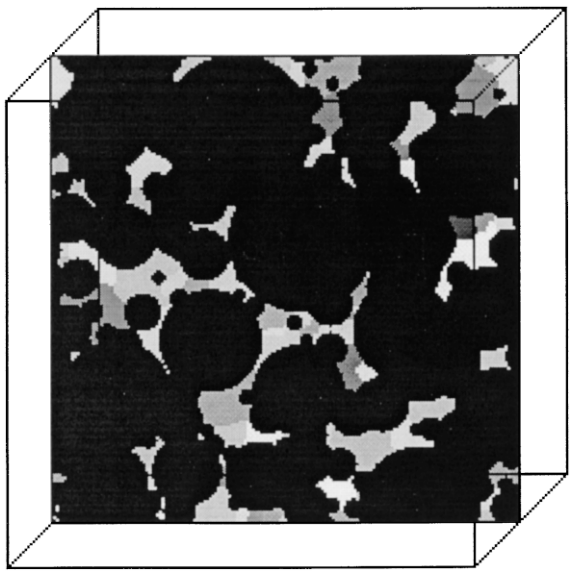

Fig. 13. Two-dimensional section in the middle of the specimen after 1 week of hydration.

the computational volume. The black color indicates the solid; for each partitioned pore a gray level is attributed.

3. Discussion and conclusion

Mercury porosimetry is used commonly to derive the pore size distribution of cement-based materials. The data are the incremental volumes of mercury that enter the pore space at each pressure increment. The interpretation of the data is difficult and the derived pore size distribution based on simple interpretation can be misleading. We computed the pore size distribution, of pores with radius ranging from 5 to 0.5 μm, of 2D and 3D images of simulated hydrated cement paste. Two different techniques were used: a mercury intrusion technique (MIT) and a morphological thinning and partitioning of void space (MTPVS). Fig. 4 shows the pore size distributions of 2D images computed by MIT, and Fig. 8 illustrates the result obtained by MTPVS on the same images. In Fig. 3, the numerical application of MIT follows a procedure similar to the real mercury intrusion test. Fig. 3 shows the maximum penetration of mercury, under a given meniscus diameter, started from the edges of the image, into the pore space. We can see that the curves in Fig. 4 can represent the pore size distribution only if the pore space is composed of nonintersecting cylindrical pores. Comparing the results given in Fig. 4 with those shown in Fig. 8 indicates strong discrepancies between curves belonging to the same images.

We applied MTPVS to determine an accurate pore size distribution of an image for later comparison with the result obtained by MIT. It should be noted that in the MTPVS technique, the shape of the cumulative pore size distribution curve depends on the definition of equivalent pore radius, but we postulate that the curves presented in Fig. 8 represent a reasonably accurate size distribution of the pores of 5 to 0.5 μm for the three selected slices. Fig. 8 shows a much smaller percentage of small pores than suggested by MIT.

We applied MTPVS directly to 3D images. To show the applicability of the technique to 3D images, 2D images of partitioned of pore space are illustrated in Figs. 11–13. For each pore a gray level is attributed for differentiation from other pores at each hydration time. The evolution of cement paste microstructure, especially the nucleation of CH in the water, changes the shape and the pore size distribution of the pores. One can observe this variation in the 2D section cut from the middle of computational volume in Figs. 11–13. The computed pore size distribution curves for cement at different hydration times are given in Fig. 9. The curves show that, during hydration, the porosity and the mean hydraulic radius decrease. There is no difference between results for hydraulic radii of 0.3 and 0.6 μm because the pixel dimension was 0.5 μm. Fig. 10 shows that the connectivity of the pore space only decreases for hydrated cement with porosity less than 10%. It is important to note that this result depends strongly on the pixel dimension. For smaller pixel dimension, the result would be more accurate. It is possible that this connectivity stays equal to one (almost all pores remaining connected even for the last hydration steps).

The comparison between the results obtained on 3D images using two different techniques may permit us to calibrate the experimental results obtained by MIT. There is no clear understanding of the description of the pore space of the cement-based materials. Our results from characterizing the pores of simulated hydrated cement indicate that in cement paste with less than 10% porosity, almost 95% of capillary pores smaller than 2-μm diameter are connected [6]. Comparing Figs. 4 and 8 indicates that the percentage of small capillary pores seems to be much less than that found using MIT.

Acknowledgments

Financial support from Foundation for Research of Swiss Cement Industry and Swiss Office for Education and Science (OFES) is gratefully acknowledged.

References

[1] D.P. Bentz, J Am Ceram Soc 80 (1) (1997) 3–21.
[2] H.M. Jennings, S.K. Johnson, J Am Ceram Soc 69 (1986) 790–795.
[3] K.V. Breugel, Simulation of Hydration and Formation of Structure in Hardening Cement-based Materials, Ph.D. Thesis, Delft University of Technology, 1991.
[4] D.P. Bentz, . J. Garboczi, Cem Concr Res 21 (1991) 325–344.
[5] P. Navi, C. Pignat, Simulation of effects of small inert grains on cement hydration and its contact surfaces, in: H.M. Jennings, J. Kropp, K.L. Scrivener (Eds.), The Modeling of Microstructure and Its Potential for Studying Transport Properties and Durability, Kluwer Academic Publishers, Dordrecht, The Netherlands, 1996, pp. 227–240.
[6] P. Navi, C. Pignat, Adv Cem Based Mater 4 (1996) 58–67.
[7] S. Bryant, G. Mason, D. Mellor, J Colloid Interface Sci 177 (1996) 88–100.
[8] C.A. Baldwin, A.J. Sederman, M.D. Mantle, P. Alexander, L.F. Gladden, J Colloid Interface Sci 181 (1996) 79–99.
[9] E.J. Garboczi, D.P. Bentz, Adv Cement Mater CeramTrans 16 (1991) 365–380.
[10] J. Hoshen, R. Kopelman, Phys Rev B 14 (1976) 3438–3445.